



Holocene floods in a complex fluvial wetland in central Spain: Environmental variability, climate and time



Juan I. Santisteban^{a,*}, Rosa Mediavilla^b, Luis Galán de Frutos^b, Ignacio López Cilla^b

^a Dpt. Geodynamics, Stratigraphy and Paleontology, Fac. of Geological Sciences, Complutense University of Madrid, C/José Antonio Novais, 12, 28040 Madrid, Spain

^b IGME, Geological Survey of Spain, C/Ríos Rosas, 23, 28003 Madrid, Spain

ARTICLE INFO

Keywords:

Flooding
Holocene
Central Spain
Western Mediterranean
Facies analysis
Geochemical indexes
Hydroclimate
Forcings

ABSTRACT

The study of flooding can be complex as it involves dynamic systems (rivers) characterized by high variability in time and space. To minimize the effects of these handicaps, we merge several records from different locations across the hydrographic basin of the Upper Guadiana River (central Spain) and use multiple proxies. The comparison of three nearby cores by means of the facies, stratigraphic correlation and geochemical indexes allows us to differentiate local environmental changes related to the natural behaviour of the system (autocyclic) from those driven by external forcings (alloycyclic). The facies and facies sequence analyses allow long-term paleohydrological trends to be reconstructed and parameters that are used to identify flooding events to be determined. Si (proxy for siliciclastic supply) and Ca/S (proxy for water budget/level) show trends that can be related to facies sequences and long-term variations. Si/Al is used as a sorting proxy (transport efficiency). To analyse the relative changes in sediment discharge and transport efficiency, these proxies are compared with water budget level, represented by (Si/Al)/(Ca/S) (sorting vs. water level) and Si/(Ca/S) (siliciclastic discharge vs. water discharge). We were able to define local, major and minor regional flood events/periods and events by relating sequence boundaries to the occurrence of environmental conditions related to high energy events (relative/absolute sorting, water level, sediment discharge) across multiple cores. Comparison to other studies around the western Mediterranean basin allows us to identify common periods of flooding at 9000–8400 cal. BP, 7700–7100 cal. BP, 6400–6200 cal. BP, 4900–3700 cal. BP, 3500–3300 cal. BP, ca. 2600 cal. BP, ca. 2000 cal. BP, ca. 1500 cal. BP and 1000–300 cal. BP. For the long-term evolution, it seems that changes in insolation during the Holocene could have played a role in controlling the hydrology. However, determining the drivers of higher-frequency variation is more challenging due to uncertainties in the chronologies and local differences. Nevertheless, some degree of correlation among these flooding periods and higher frequency changes in irradiance, temperature and NAO is observed.

1. Introduction

While there remains limited evidence of increasing magnitude or frequency of floods, their impacts are expected to increase as the number of people potentially affected by flooding is growing (Hartmann et al., 2013; Jiménez-Cisneros et al., 2014). Consequently, enhancing our knowledge about the factors that trigger floods and how often they happened in the past is crucial and can help in the management and planning of human activities around fluvial basins. Further study is therefore needed to look for patterns, cyclicities and/or thresholds, improve chronologies and identifying forcings that could enhance our ability to forecast their future behaviour.

However, there are still many sources of uncertainty: our

documentary records are incomplete, flooding episodes are spatially heterogeneous, major floods or periods of intense flooding can destroy the imprint of earlier floods, many of our proxies average “flooding” and “non-flooding” periods making difficult to identify or determine the magnitude of individual floods or flooding periods, our understanding about the environmental variability and forcings is not complete and the chronologies are not perfect (Faust and Wolf, 2017).

One of the first questions to answer is: what's a flood?

In Article 2 of the Directive 2007/60/EC on the assessment and management of flood risks, “‘flood’ means the temporary covering by water of land not normally covered by water” (European Union, 2007). According to the National Flood Insurance Program of the USA: “Flood. A general and temporary condition of partial or complete inundation of

* Corresponding author.

E-mail addresses: j.i.santisteban@geo.ucm.es (J.I. Santisteban), r.mediavilla@igme.es (R. Mediavilla), l.galan@igme.es (L. Galán de Frutos), i.lopez@igme.es (I. López Cilla).

<https://doi.org/10.1016/j.gloplacha.2019.102986>

Received 31 December 2018; Received in revised form 11 May 2019; Accepted 29 June 2019

Available online 02 July 2019

0921-8181/ © 2019 Elsevier B.V. All rights reserved.

2 or more acres of normally dry land area or of 2 or more properties” (<https://www.fema.gov/national-flood-insurance-program/definitions#F>). But these definitions are based on risk and focused on human activity. In fact, from a sedimentological point of view, flooding is one of the intrinsic mechanisms of the fluvial systems. Thus, it's a “normal” process in nature but a risk for humans.

To manage this dichotomy, we look for criteria to identify what is “common” and what is an “event”. These criteria can involve the analysis of the extent of the flooding and its magnitude and frequency. But the variability of fluvial systems in time and space introduces complexities to such analysis. The fluvial system comprises laterally finite subenvironments that change suddenly and fluctuate between periods of no activity, instances of flooding that leaves deposits (aggradation) in the channels and adjacent areas and other times when fluvial energy is sufficiently high that it erodes previous deposits. (Zielhofer and Faust, 2008; Benito et al., 2008, 2015a,b).

Floodplain wetlands are present all around the world and inundation of floodplains by a combination of surface water (river) and groundwater is not usual (Bradley, 1997). Examples of this kind of wetland can be found in Ireland (Heery, 1993), Germany (Köhler, 1993), Nigeria (John, 1986), Botswana (Allanson et al., 1990), South Africa (Tooth et al., 2007; McCarthy et al., 2011; Larkin et al., 2017), Irak (Richardson et al., 2005), Australia (Hesse et al., 2018) and in South America (Junk, 1984; Hamilton and Lewis, 1990; Carignan and Neiff, 1992). Most of the mentioned fluvial wetlands correspond to humid wetlands. Mertes (1997) and Lewin and Ashworth (2014) consider that floodplain wetlands are the result of channel processes (avulsion, displacement, etc.) and wetlands with disconnected channels or related to hyporheic waters are characterized by scarce clastic sedimentation.

Dry wetlands are quite different to humid ones as they suffer more frequent/longer desiccation periods, channels decrease in size downstream, chemical sedimentation is more important, fires play a role in the preservation of organic matter and they show longer timescales of development (Tooth and McCarthy, 2007). McCarthy et al. (2011) revealed that the Nyl River floodplain wetland in South Africa developed via blocking of the main trunk by tributary coarse grain alluvial fans. This promoted backponding, gradient reduction and sedimentation. Larkin et al., 2017 analysed the Tshwane-Pienaars floodplain wetlands (South Africa) and their relation to extrinsic and intrinsic factors. They showed that the presence of resistant rocks provides a base level of the Pienaars River, which controls ponding and valley widening upstream. They propose that greater aridity increases the ratio of sediment input/output from the wetland, enhancing the discontinuity of channels and floodout.

In this paper, we analyse the flooding history of a Spanish floodplain wetland that shares some features with these examples. The wetland is located upstream of a bottleneck made of metamorphic rocks and at the junction of two rivers. Along with the karst-induced subsidence, this promotes backponding and sedimentation (infilling). Climate is semi-arid and groundwater fluctuations play a role in cyclical ponding as, under natural conditions, the wetland is a groundwater discharge area (Mertes, 1997; Winter, 1999). We present an environmental interpretation of the facies, stratigraphic correlation and geochemical content to establish a hierarchy of flooding events (from local to regional and interbasinal) at different time scales. Finally, we discuss possible forcings that could be linked to the evolution of the interbasinal events.

1.1. Location and geological setting

The study area is in the Southern Spanish Meseta, in the Upper Guadiana River basin, near the confluence of the Gígüela and Guadiana-Azuer rivers that supply the sediments that fill the fluvial basin (Fig. 1) as solids (siliciclastics) and solutes (sulphate and carbonate). The physiography and water quality of these rivers are very different. The Gígüela River is characterized by a very flat and wide

valley draining from the ENE and fed by rivers draining, among other rocks, saline materials of Triassic age, which makes its water's sulphate-rich. The Guadiana-Azuer River flows through relief composed of carbonates in the SE study area and it shows higher slopes, more encased valleys and supplies carbonate-rich waters.

The southern margin rests upon Pliocene karstified carbonates, the northern margin is bounded by Plio-Pleistocene siliciclastic deposits and, downstream, the basin is closed by metamorphic rocks of Paleozoic age. Additionally, there are some volcanic rocks of Plio-Pleistocene age. The fluvial landscape is controlled by the geology of the region. Thus, the karstification-related subsidence, a highly-resistant (metamorphic) “bottleneck” and near-surface groundwaters are responsible of the encased morphology of the fluvial valley, its low lateral mobility, and its infilling trend. These characteristics in turn determine the low gradient of the fluvial system and its hydrodynamics (Mediavilla et al., 2013).

The Quaternary infill of the basin is mainly composed, to the N, of Plio-Pleistocene alluvial fan deposits and, to the S, Pleistocene fluvial deposits of siliciclastic nature. The Holocene record is diverse and, in the studied area, is made of siliciclastics (fluvial), carbonates and organic rich muds (fluvial wetland) (Mediavilla et al., 2013).

The Holocene infill is a complex body typically composed of fluvial deposits (channel-floodplain systems) that change upwards and laterally into fluvial wetland deposits (Fig. 2) (Santisteban et al., 2004; Domínguez-Castro et al., 2006; Mediavilla et al., 2013; Santisteban et al., 2017a). Channel-floodplain systems were dominant during the Pleistocene and beginning of the Holocene and some local episodes of fluvial wetland development took place at the end of the Pleistocene. But from mid-Holocene onwards, the fluvial wetland expended upstream reaching its maximum development around mid-20th century CE.

The Quaternary sediments are arranged in three units bounded by erosive surfaces related to fluvial reactivation episodes. The lowermost (Late Pleistocene 2, Fig. 2) is a fluvial sequence encased on Paleozoic and Pliocene rocks and represents a final wetland episode. This unit is cut by the following unit (Late Pleistocene 1) that is deeply encased in the previous deposits (reaching the Paleozoic substratum). The third unit (Holocene) is encased in the previous one and records the spreading of the wetland environment. This unit shows some bounding surfaces that can be related to fluvial reactivation episodes and to flooding-drying cycles.

Human settlements have been present in the surroundings of the fluvial system since the Neolithic, but humans did not severely modify the fluvial system until the late 18th c. CE and more intensely since the second half of the 20th c. CE (Celis et al., 2017).

1.2. Climate, hydrology, wetland and flooding

The climate at the study area is characterized by warm, dry summers and cold winters, with most rainfall concentrated from October to May. The average annual temperature for the period 1904–2012 is 14.6 °C and average annual rainfall is around 407 mm. Minimum-maximum monthly average values range from −5 °C to 33 °C and from 0 mm to 220 mm (Santisteban and Mediavilla, 2013).

An analysis of climate for the 1904–2012 period reveals that dry and wet periods alternate in asymmetrical cycles. Wet periods of 6–7 years were followed by dry periods of 3–4 years composed by smaller dry-wet cycles of 3–5 years in which the “dry” interval is longer. Until the 1930s, these cycles were centred on an average level and showed a moderate amplitude, that widened until the 1980s. From that time until present, there is a trend towards more arid conditions (Santisteban and Mediavilla, 2013).

These cycles controlled the natural evolution of the fluvial system and the wetland water table extent until the second half of the 20th c. CE, when desiccation works, intensive irrigation and damming of the rivers began modifying the hydrological cycle (Santisteban and

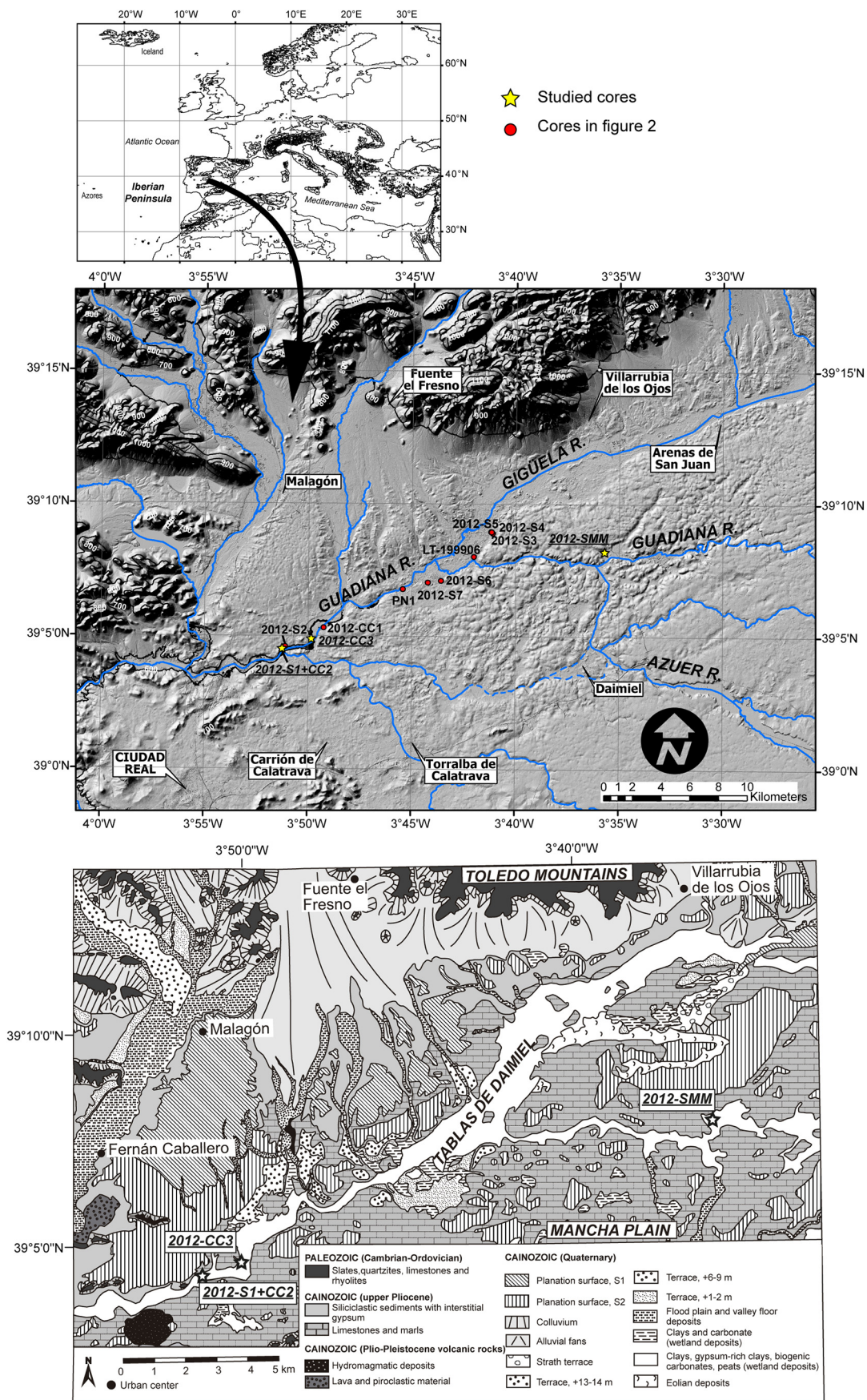


Fig. 1. Geographical location and geological setting of the study area. The shadowed relief model shows the present drainage network and the location of the studied cores (river flow is towards the west). A geological sketch of the same region (modified from Portero et al., 1988; Rodríguez-García, 1998; Hernández et al., 2013; Rey et al., 2017). The topographic information and aerial photographs have been provided by the Spanish Geographical Institute (IGN) and the river courses by the Guadiana Water Authority (CHG).

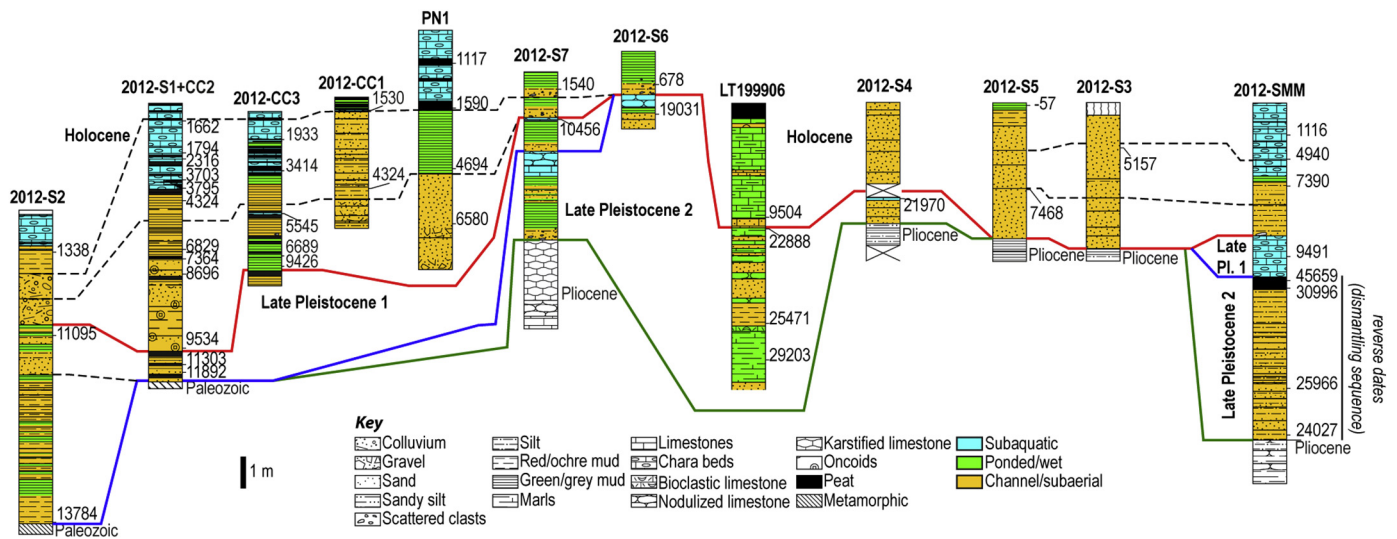


Fig. 2. Stratigraphic framework of the Late Pleistocene-Holocene infill of the studied area (modified from Santisteban et al., 2017a). Calibrated radiocarbon ages are placed to the right of the stratigraphic sections.

Mediavilla, 2013; Celis et al., 2017). However, most of the natural features of the system can be observed in surface, outcrops or underground by means of cores (Santisteban et al., 2004) or geophysical techniques (Rey et al., 2017).

The Guadiana-Azuer-Gigüela floodplain wetland is characterized by channels with a high width/depth ratio, defined in those areas where the valley narrows enough to concentrate the flow. Channels in river are less well-defined, or their margins are mobile fringes or islands composed by vegetation (dominated by *Typha*, *Cladium* and *Phragmites*). The out-channel (floodplain) areas are mostly shallow karstic closed depressions, lying below the channel level and bounded from the valley margin and the channels by hydrophyte stripes. Some of these depressions show springs inside.

The hydrodynamics of the system is regulated by the position of groundwater in relation to the surface and the frequency of surficial flooding, resulting in complex interactions (Winter, 1999). During dry periods, the groundwater drops below the surface, the open water areas decrease or disappear, and marginal vegetation expands inside the wetland. Surface waters supply clastic material that is trapped by vegetation or accumulates on the surface during individual floods. Gypsum forms by evaporation during the low-water stages (Fig. 3). During wet periods, the groundwater level (at regional scale) rises above the ground surface causing the development of semi-permanent flooded areas, Charophycea mats develop at these areas during non-flooding episodes, while the marginal vegetated fringe retreats outwards. During flood episodes, most clay is washed downstream from the open water areas while silt and sand are deposited upon the Charophycea mats (not growing due to turbidity), and the whole detrital load is trapped at the vegetated margins (Fig. 3).

Thus, flooding happens at different time scales and hydrological stages: a) Long-term, cyclic, regional, flooding results from wet periods and rising of the groundwater table resulting in the development of open water facies (calcite), b) individual surface floods, local or regional, can leave their imprint as higher siliciclastic input events during these high-water stages; c) dry periods imply the desiccation of the wetland and only individual surface floods, local or regional, are recorded by peaks of siliciclastic supply without evidence of rising water tables but a signal of water budget deficit (increase in gypsum) is observable. As groundwater rise results on long-term flooding (decennial to centennial), this flooding won't be considered in the present study.

2. Methods and materials

2.1. Coring and core analysis

During the coring campaign of December 2012, 8 rotary cores (named 2012-S1, S2, S3, S4, S5, S6, S7 and SMM) and 3 vibracores (named 2012-CC1, CC2 and CC3) with continuous recovery were obtained at 10 sampling points in the studied area. Vibracore 2012-CC2 was taken to complete the upper part of core 2012-S1 as the recovery was so poor. In addition, older cores from other studies were considered to complement the stratigraphic information (PN-1, de Bustamante et al., 1995, and LT199906, Valdeolmillos, 2005).

Detailed stratigraphic sections were corrected for depth (to account for compaction during the drilling) and sampled for geochemistry and mineralogy. Additionally, 50 samples were taken for ¹⁴C AMS dating to help in the correlation of the cores (Fig. 2).

Cores 2012-S1, CC2, and SMM were chosen as all the sedimentary facies are visible and they record almost the entire Holocene. These cores were split and analysed for:

- 1) 1 mm sample spacing colour scan (Geoscan IV Geotek ©);
- 2) continuous geophysical scan, 5 mm sample spacing, for sonic, density, resistivity and magnetic susceptibility (MSCL Geotek ©);
- 3) geochemical scan, 10 mm sample spacings, for 10 kV and 30 kV with an Itrax Core Scanner (data processed with Itrax proprietary software) at the University of Barcelona facilities, for cores 2012-SMM, S1 and CC2, and with the XRF Geotek of the laboratories of the Spanish Geological Survey, for core 2012-CC3 (data processed with bAxil);
- 4) continuous sampling with 10 mm thick samples for the uppermost meter of the core and 20 mm thick samples for the rest of the core: One of each five of these samples was split for ICM-MS and ICP-AES geochemical analysis to check the geochemical scan results, total C and S in an elemental analyser (Leco © SC-444DR), inorganic C by colourimetry (UIC © CM140), with organic C being the difference between the total and inorganic C, and N (NH₄, Technicon Autoanalyser ©, and NO₃, colourimetry CTA Method).

The mineralogy was analysed at the Spanish Geological Survey by XRD for the bulk sample and the < 20 µm fraction to correlate with the geochemical composition.

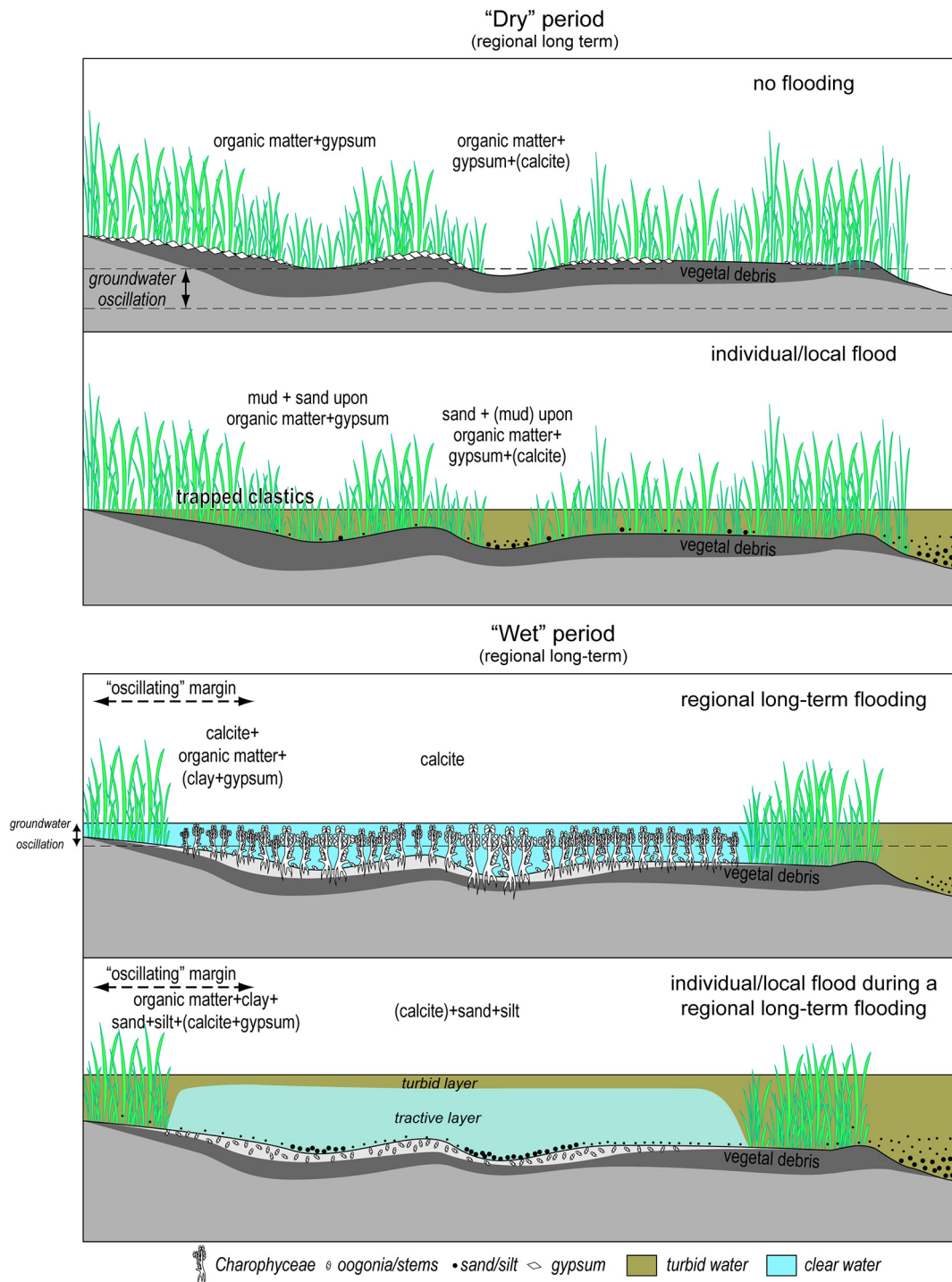


Fig. 3. Flooding scenarios in the fluvial wetland and recorded products. In this study, regional long-term flooding related to groundwater rise won't be considered.

2.2. Facies and environments

The facies represented in the cores correspond to two main groups of fluvial (s.l.) origin:

- a) Fluvial facies characterized by the presence of defined channels and floodplain and
- b) fluvial wetland facies resulting from slowly moving waters downstream without well-defined channels but with "islands" composed by hydrophytes that moved through time in response to the fluctuations of the water table (Santisteban et al., 2004).

These facies groups are composed of:

Fluvial facies:

- (a) Carbonate-filled channels: Oncolite gravels with a siliciclastic sandy to silty matrix. The oncolites show irregular shapes varying from spherical to elongated and a maximum length from 2 to 15 mm. Their nucleus can be a grain of sand, a charophyte remain or a fragment of a gastropod shell, and the laminae are composed of calcite. The siliciclastic matrix is composed of clays (illite), quartz and traces of feldspar. This facies could not be scanned for geochemistry as its surface was too rough to obtain

reliable data. The features of these deposits point to running waters in a confined body but not too energetic as the oncolites are well rounded and preserved. Rey et al. (2017) interpret them as channel facies by their internal structure in the geophysical profiles. These sediments used to be covered by channel plug facies (see below).

- (b) Siliciclastic channels: Massive sands to laminated or massive muds with variable amounts of sand and clay and fossil remains (fragments of gastropods, plants and charophytes). Their colour is pale green or pale brown and their mineralogy is composed of clay (illite and kaolinite), quartz, calcite, and traces of feldspar and gypsum. Root traces are common. They can be filling erosive surfaces or lying upon other channel facies forming fining upwards sequences with floodplain and channel plug facies. Rey et al. (2017) identified in their geophysical profiles internal erosive surfaces and lateral accretion units that allow to interpret them as channel facies.
- (c) Floodplain: Massive dark-brown to black organic-rich muds with very variable content of sand, clay and fossil remains (unbroken shells and fragments of gastropods and vegetal remains). They can contain up to 10% organic matter, while other components are clay, quartz and calcite, and traces of feldspar and gypsum. They are positioned laterally or upon the channel facies in the geophysical profiles of Rey et al. (2017) and by their content can be interpreted as densely vegetated floodplains.

Wetland facies:

- (d) Open wetland: Whiteish to cream sand and silt composed of charophyte remains (stems and oogonia) with variable amounts of organic matter, siliciclastic components and gypsum (all of them always in low amounts). Their mineralogy is composed of calcite, clay (illite), quartz, and traces of gypsum and aragonite. Santisteban et al. (2004) interpret them as deposits resulting from the in situ accumulation of charophytes in open water bodies where water runs slowly and there were no macrophytes. They used to be covered by open wetland margin deposits (see below).
- (e) Open wetland margin: similar to the previous facies but it shows higher content in organic matter and/or mud. For that reason, its colour is greyish to brown. Their origin is similar to the previous facies but they represent locations near the margins of the wetland or the inner island where emergent vegetation grew (Santisteban et al., 2004). They are followed by wetland margin deposits (see below).

Mixed-origin facies:

- (f) Channel plug or wetland margin/islands: Massive dark brown to black peat. The organic matter (of vegetal origin) can reach up to 20%. The rest of the components are mainly clay, some quartz and gypsum in variable amounts (up to 17%). Calcite can be a main component when these sediments contain gastropod shells. They formed in wet areas where hydrophyte/hygrophyllous vegetation developed but near surface water supply (siliciclastic content) and are episodically exposed (gypsum). Depending on their position in the sedimentary sequences these conditions are interpreted as the infill of abandoned channels (channel plug) (Rey et al., 2017) or vegetated areas ("islands") or at the margins of the fluvial wetland (Santisteban et al., 2004).

Fluvial facies groups usually dominate the lower portion of the sections while the fluvial wetland facies are widespread towards the top but there is a lateral change among them by means of the wetland margin and floodplain facies (Figs. 2, 4). Domínguez-Castro et al. (2006) analysed some cores upstream and stated that wetland sedimentation expanded upstream until the 20th century CE when fluvial sedimentation was gradually restricted to upstream reaches and valley side areas.

2.3. Age models and time resolution

AMS ¹⁴C dating of samples was done at the GADAM Centre (Gliwice, Poland). 26 bulk samples were analysed as all potential C sources were biological (vegetal remains and bio-induced carbonates). The selection of samples was determined by their stratigraphic position and lack of evidence of contamination. Dates were calibrated by CALIB 7.1 (Stuiver and Reimer, 1986, 1993; Stuiver et al., 2015), using the IntCal 13 curve (Reimer et al., 2013) (Table 1).

Comparison of the age-depth curves led to two samples being rejected owing to old C contamination and three samples showed age reversals that interrupted the sequence. The age-depth model (Fig. 5) was constructed from the remaining dates and tested by correlation of stratigraphic facies and geochemical peaks and trends. A good indication of the quality of the material was the fact that only minor adjustments were made to the age-depth model and these were probably related to the linear nature of the thickness correction method, which does not allow for inhomogeneity in the lithology. In addition, the sedimentation rates are consistent among cores and areas and only the charophyte carbonate from Tablas-2012-SMM core shows lower sedimentation rates that can be related to local factors: charophyte beds: 0.20–0.80 mm/yr with more common values around 0.5–0.6 mm/yr; fluvial mud: 0.51–0.72 mm/yr but can be as low as 0.15 mm/yr; channel deposits: 1.04–1.1 mm/yr.

According to these age models, the statistics for the time span covered by the samples are: mean: 23.15 years (2012-S1 + C2 = 22.98, 2102-CC3 = 27.43, 2012-SMM = 19.45), mode: 13.4 years (2012-S1 + C2 = 13.03, 2102-CC3 = 25.21, 2012-SMM = 13.39), standard deviation: 17.32 years (2012-S1 + C2 = 10.93, 2102-CC3 = 15.67, 2012-SMM = 23.19), maximum value: 126.28 years (2012-S1 + C2 = 60.73, 2102-CC3 = 75.64, 2012-SMM = 126.28), minimum value: 4.77 years (2012-S1 + C2 = 6.75, 2102-CC3 = 12.21, 2012-SMM = 4.77).

2.4. Geochemical proxies

The sedimentation is dominated by material from the low slopes of that Gígüela River and the Guadiana-Azuer rivers. The supply of both rivers is buffered/filtered by the wetland, so the sedimentation is dominated by low energy siliciclastic sediments (clay + silt + fine sand) and/or authigenic sediments. Another constraint is that, due to the sampling resolution, a single sample can record one or several floods and, therefore, the record can represent the strongest peak of a single flood or the average of different floods. Assuming that a single flood is a high transport efficiency and water discharge event, it should be characterized by higher sediment discharge, but its transport efficiency is related to the flow velocity which, in turn, depends on the water discharge and the roughness of the flow path. This will be conditioned by the density of the hydrophyte cover, being lower during the wet periods and higher during the dry periods. Thus, a single flood during a dry hydroperiod will be characterized by high sediment discharge and poor sorting while during a wet period the sorting will be better for a similar water discharge but can be poorer if the water discharge is lower. So, to interpret the record, we use the solid (siliciclastic) sediment discharge, which relates to water discharge (flood peak), the sorting of the solid (siliciclastic) sediment, which depends on the settling velocities and the flow velocity, and the water level, related to wet or dry hydroperiods.

In this study, we use Si, an element shared by all siliciclastic components, as a proxy of the total siliciclastic discharge. As the sediment is dominated by the fine grain size fractions, the clay composition is homogeneous, the amount of feldspar is negligible, and Al is present in phyllosilicates but not in quartz, the Si/Al ratio reflects the quartz/clay ratio. It can therefore be used as an indirect sorting proxy ($[\text{sand} + \text{silt} + \text{clay}]/\text{clay} = [(\text{sand} + \text{silt})/\text{clay}] + 1$) (Viscosi-Shirley et al., 2003; Calvert and Pedersen, 2007; Ohta, 2008; Dhivert et al., 2015).

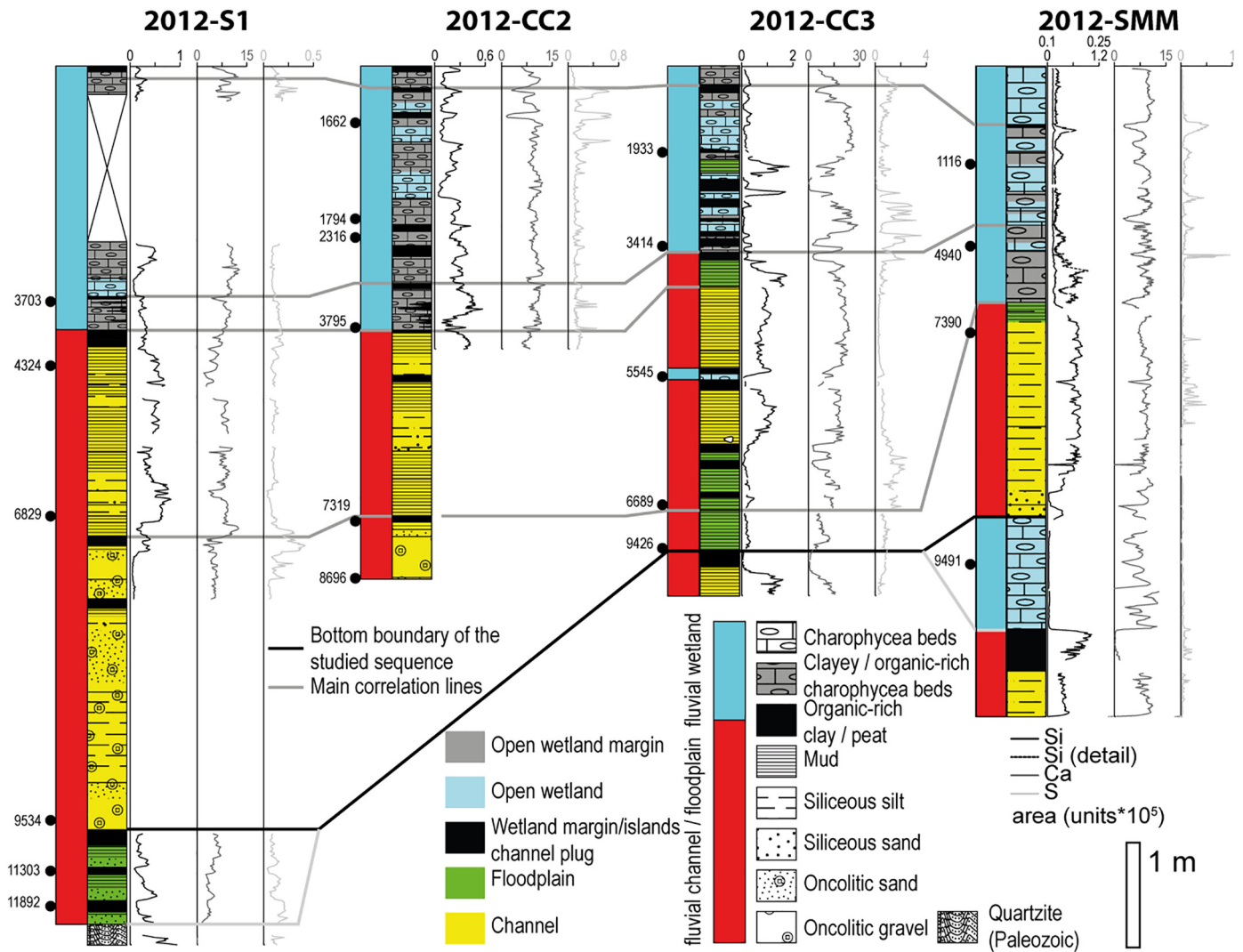


Fig. 4. Facies, geochemical basic information, dates (numbers at the left side of the cores are yr cal. BP) and main correlation lines of the studied cores.

Water level can be derived from authigenic sediments, calcite and gypsum. Calcite is related to fresh-water dominance while gypsum is linked to water deficit (evaporation). Ca is shared by carbonate and gypsum while the only source of S is gypsum. Consequently, the Ca/S ratio provides information about the changes in the (calcite + gypsum)/gypsum ratio, which is related to the fresh/saline waters ratio ($[\text{fresh} + \text{saline}]/\text{saline water} = 1 + [\text{fresh}/\text{saline}] \text{ water}$). This, in turn, reflects the water budget (water inputs vs. evaporation losses) and, indirectly, high (more fresh water input or less evaporation) vs. low (more evaporation) water stages.

However, the use of ratios introduces the handicap that they record relative rather than absolute magnitudes. To minimize this effect, we combine different ratios to scale the values. In our case, we scale the transport proxies (sediment discharge, Si, and the transport efficiency, Si/Al) by means of the water level (Ca/S). The resulting indexes are sorting (transport efficiency) vs water level ($[(\text{Si}/\text{Al})/(\text{Ca}/\text{S})] = [\text{Si} * \text{S}]/[\text{Ca} * \text{Al}]$) and sediment supply (surface water discharge) vs. water level ($(\text{Si}/[\text{Ca}/\text{S}] = [\text{Si} * \text{S}]/\text{Ca})$) ratios that provide information about relative changes in energy according to the local environmental conditions or the hydraulic stage.

The studied records show clear differences both in facies distribution (lateral facies changes) and geochemical information (dependence on mineral composition of facies), but some commonalities arise (Fig. 6). It's evident that energy peaks are not dependent on sediment supply rate or water depth. They are more evident as the lithological/

mineralogical contrast is wider (i.e. siliciclastics vs. carbonates) or at low energy environments (higher energy contrast).

3. Results and discussion

To identify flood events in our sedimentary and geochemical record, two main questions must be taken into account: 1) are the proxies we analyse the result of hydrodynamic processes and/or hydrological changes that result from environmental variability (facies shifts) or out-of-sequence events?; and 2) does our chronology provide a precise date for individual events and how sure can we be that we are seeing a single event or the time averaged sum of events?

So, we must answer these two questions to provide a reliable reconstruction of the flooding history.

3.1. Local vs. regional periods (autocyclic vs. allocyclic forcings)

One of the main points of this study is to use different cores in different settings to analyse the spatial variability, the effects of the environmental variability and to use several proxies to check the validity of the inferences (coincidence of independent proxies) and the variability through time.

According to Walther's Law, in a continuous sedimentary sequence (without discontinuities), "the various deposits of the same facies-area and similarly the sum of the rocks of different facies-areas are formed

Table 1

Radiocarbon dates for cores Tablas-2012-S1 + CC2 (samples 2012-S1 and 2012-C23), Tablas-2012-CC3 and Tablas-2012-SMM.

Lab code	Sample code	¹⁴ C age	2σ cal range BP (probability)	cal range BP median probability
GdA-4767	2012-S1-258-259	3445 ± 30	3633–3782 (81.1%)	3703
GdA-3600	2012-S1-366-368	3878 ± 27	4235–4415 (99.4%)	4324
GdA-3601	2012-S1-496-498	5990 ± 25	6771–6892 (93.4%)	6829
GdA-3772	2012-S1-780	8565 ± 40	9480–9563 (97.3%)	9534
GdS-1742	2012-S1-868-870	9840 ± 160	10,740–11,826 (99.0%)	11303 ^a
GdA-3609	2012-S1-870A	10,191 ± 40	11,747–12,069 (98.9%)	11892 ^a
GdA-3610	2012-C23-12	3479 ± 26	3690–3833 (97.2%)	3759
GdA-4768	2012-C23-73-47	2280 ± 30	2301–2351 (63.2%)	2316
GdA-3611	2012-C23-102	1859 ± 24	1725–1866 (100%)	1794
GdA-3612	2012-C23-128	1762 ± 21	1610–1726 (100%)	1662
GdA-3613	2012-C23-443	6332 ± 29	7230–7318 (78.2%)	7264
GdA-3614	2012-C23-487	7898 ± 31	8596–8786 (90.1%)	8696
GdA-4769	2012-CC3-78-79	1985 ± 25	1885–1990 (100%)	1933
GdA-4770	2012-CC3-179-180	3190 ± 30	3361–3459 (100%)	3414
GdA-3608	2012-CC3-295-297	4827 ± 27	5478–5536 (50.9%)	5545
GdA-4771	2012-CC3-419-420	5865 ± 35	6618–6756 (94.9%)	6689
GdS-1744	2012-CC3-464-465	8450 ± 180	8995–9920 (99.4%)	9426
GdA-3774	2012-SMM-41-42	1183 ± 26	1053–1180 (96.2%)	1116
GdA-4766	2012-SMM-188	26,880 ± 115	30,796–31,181 (100%)	30996 ^c
GdA-3775	2012-SMM-207-208	4387 ± 29	4866–4988 (80.4%)	4940
GdA-4765	2012-SMM-229	23,020 ± 110	27,106–27,563 (100%)	27348 ^c
GdA-3776	2012-SMM-268-269	6487 ± 32	7322–7444 (97.3%)	7390
GdA-3777	2012-SMM-450-452	8466 ± 37	9440–9531 (100%)	9491
GdA-3778	2012-SMM-550-552	42,370 ± 625	44,535–46,861 (100%)	45659 ^b
GdA-3779	2012-SMM-900-902	21,718 ± 156	25,685–26,277 (100%)	25966 ^b
GdA-3780	2012-SMM-1061-1063	19,971 ± 138	23,663–24,370 (100%)	24027 ^b

^a Dates corresponding to the late Pleistocene 1 sequence.

^b Dates corresponding to the late Holocene sequence in a dismantling sequence.

^c Rejected ages (reworked carbon).

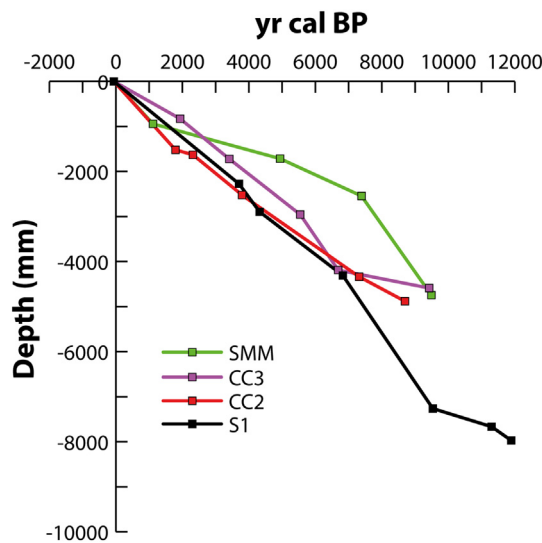


Fig. 5. Age models for the studied cores.

beside each other in space, though in a cross section we see them lying on top of each other. As with biotypes, it is a basic statement of far reaching significance that only those facies and facies-areas can be superimposed primarily which can be observed beside each other at the present time" (Walther, 1894, translation by Middleton, 1973).

Then, these continuous facies sequences are interpreted in terms of environmental variability due to intrinsic (autocyclic) or extrinsic (alloycyclic) factors. If we consider that tectonic activity in this area is slower than the duration of the normal sequences, differentiating what changes are driven by climate action or natural displacements of the system becomes key. In this sense, we must consider that the natural displacements of these systems result in the concurrent development of opposing sequences (i.e. shallowing-upwards vs. deepening-upwards, fining-upwards vs. coarsening-upwards, Fig. 7a) while a change in

energy of the system (i.e. change in water supply or slope) is recorded as similar trends along the system (Fig. 7b).

Consequently, simultaneous increases of energy (as recorded by increases in sorting or sediment supply) under similar water levels recorded in both areas will be considered as representing a regional major flood episode or period. Additionally, regional increases in energy coeval with different trends in water level represent regional floods resulting in channel shifts (lower energy). On the other hand, noticeable increases in water energy recorded in both 2012-S1 + CC2 and 2012-CC3 or in 2012-SMM will be interpreted as local floods affecting the Gigüela River sub-basin (2012-S1 + CC2 and 2012-CC3) or the Guadiana-Azuer rivers sub-basin (2012-SMM) (Fig. 8).

3.2. Time scales, hydroclimate and flooding periods

According to our age models, individual samples represent at least several years, so we cannot guarantee that the recorded changes correspond to a single flood or multiple events (flooding periods) within that time window. In addition, the presence of local maxima in the flood proxies from different cores showing similar ages supports their interpretation as flooding periods instead of flood events (Fig. 8).

The time extent of these periods varies from several years-decades, in the case of the sample time scale, to the centennial to millennial scale, in the case of long-term environmental shifts or encasement cycles. In the latter situation, the main sequence boundaries (Fig. 2), like the one bounding the studied sediments, are related to the highest intensity periods of fluvial activity. During these periods, erosive surfaces are carved, encasing the following sequences into the previous units (including the basement). They are linked to millennial time scales. The shorter sequences (facies sequences) are bounded by low-water stage deposits. After the relative drying of the environment, flooding must occur to develop the next sequence. In the case of fluvial deposits, the flooding can be represented by minor erosive surfaces or sudden placement of more energetic deposits. In the wetland stage/system, during the low-water stage, floods can occupy the whole area of sedimentation, and are covered by open water-type deposits. Thus, it is common to find

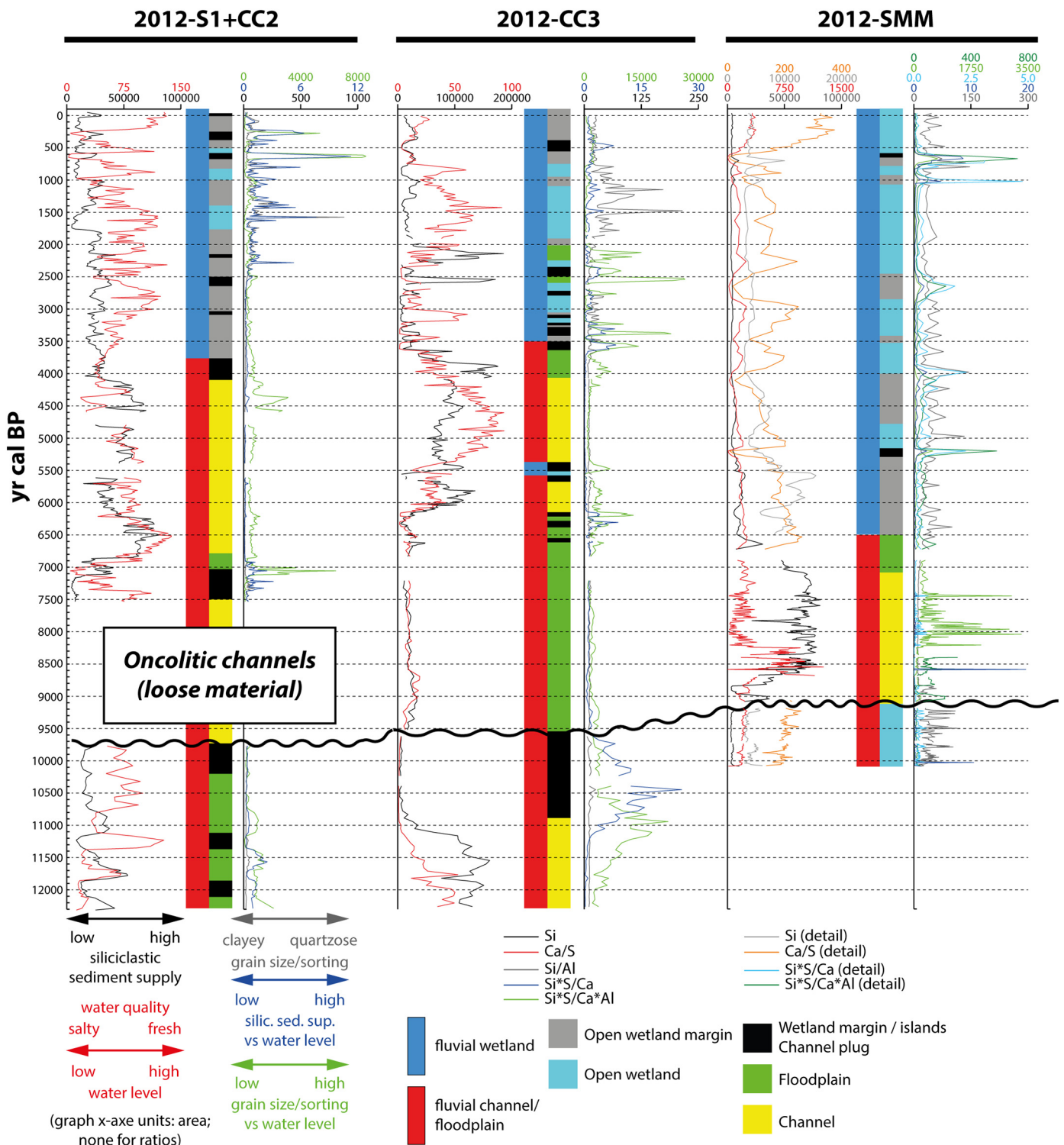


Fig. 6. Geochemical proxies and indexes on the time-scale. The undulated line marks the bottom of the Holocene sequence. The scale has been increased for the upper part of the section 2012-SMM to avoid the dominant signal of Ca.

pairs of floods related to the dry/low-water stage deposits (lower sequence) and, occasionally, to the wet/high-water stage ones. Consequently, regional flooding episodes are common at the facies sequence boundaries (Fig. 8).

The shorter periods (those contained by individual samples) are placed into the sequences and represent floods related to annual to decennial periods. They can be related both to high and low water stages as they represent minor events inside a trend. Some minor energy

regional floods and local floods fit in this category.

Analysing the distribution of the flooding proxies indicates that a more intense episode of regional flooding occurred around 9700 to 9300 cal. BP, when the erosive surface that bounds the Holocene sequence was carved. After this period, fluvial channel-floodplain systems developed all along the region, without evidences of anomalous high energy events except around 8900 cal. BP and 7100 cal. BP, when the transition to the fluvial wetland began at the Guadiana-Azuer sub-

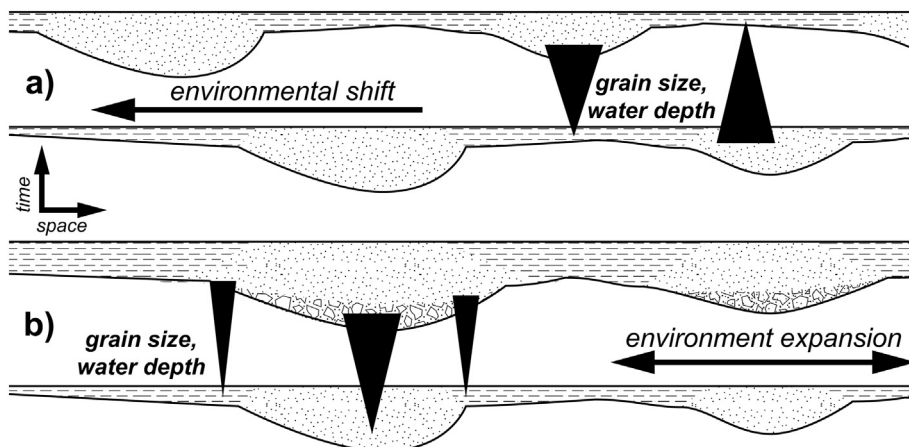


Fig. 7. Idealized scheme to represent the trends resulting from a) lateral shift of environments (i.e. autocyclic behaviour) and b) regional changes in the hydroclimate or regional slope (i.e. allocyclic forcings).

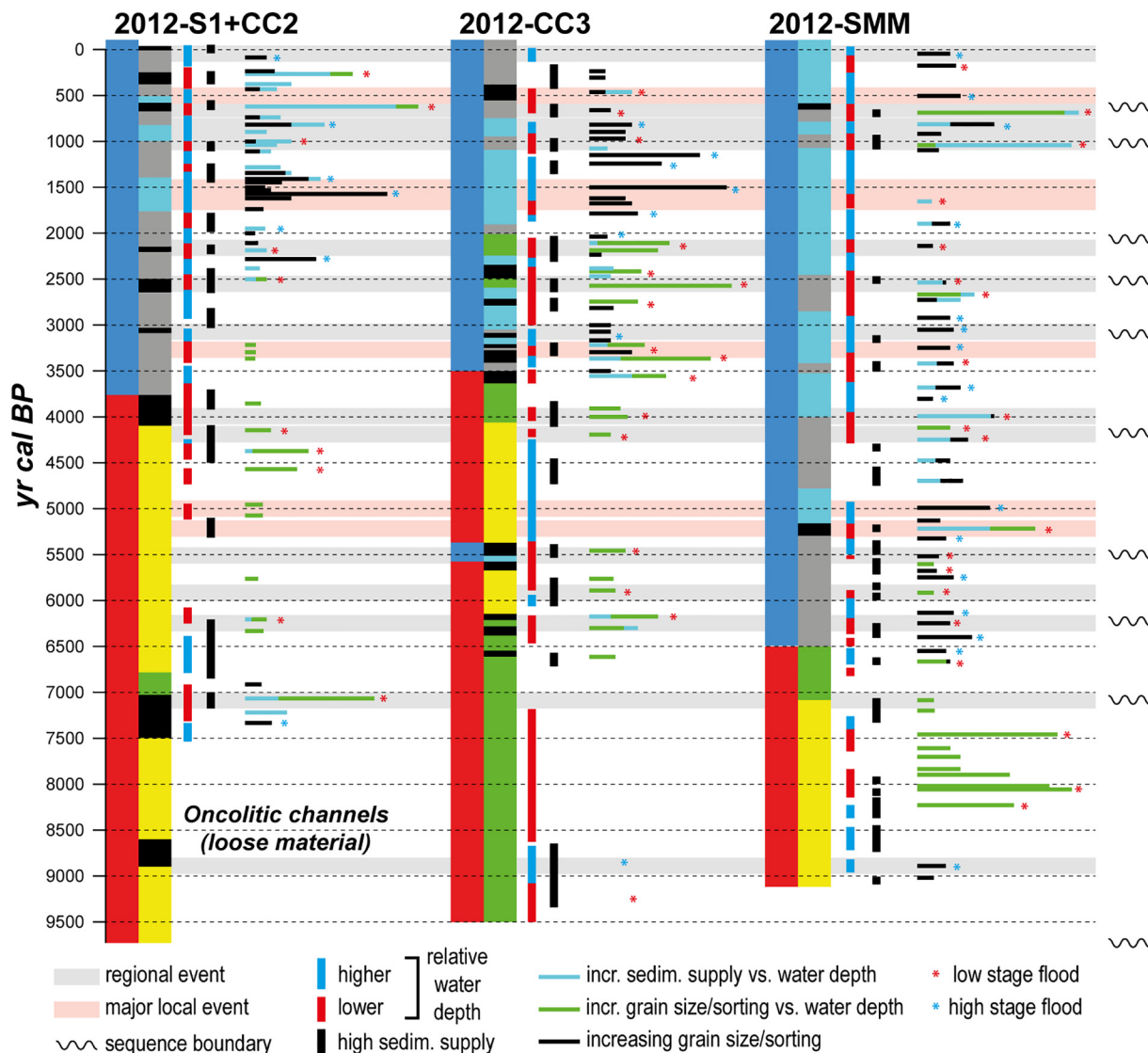
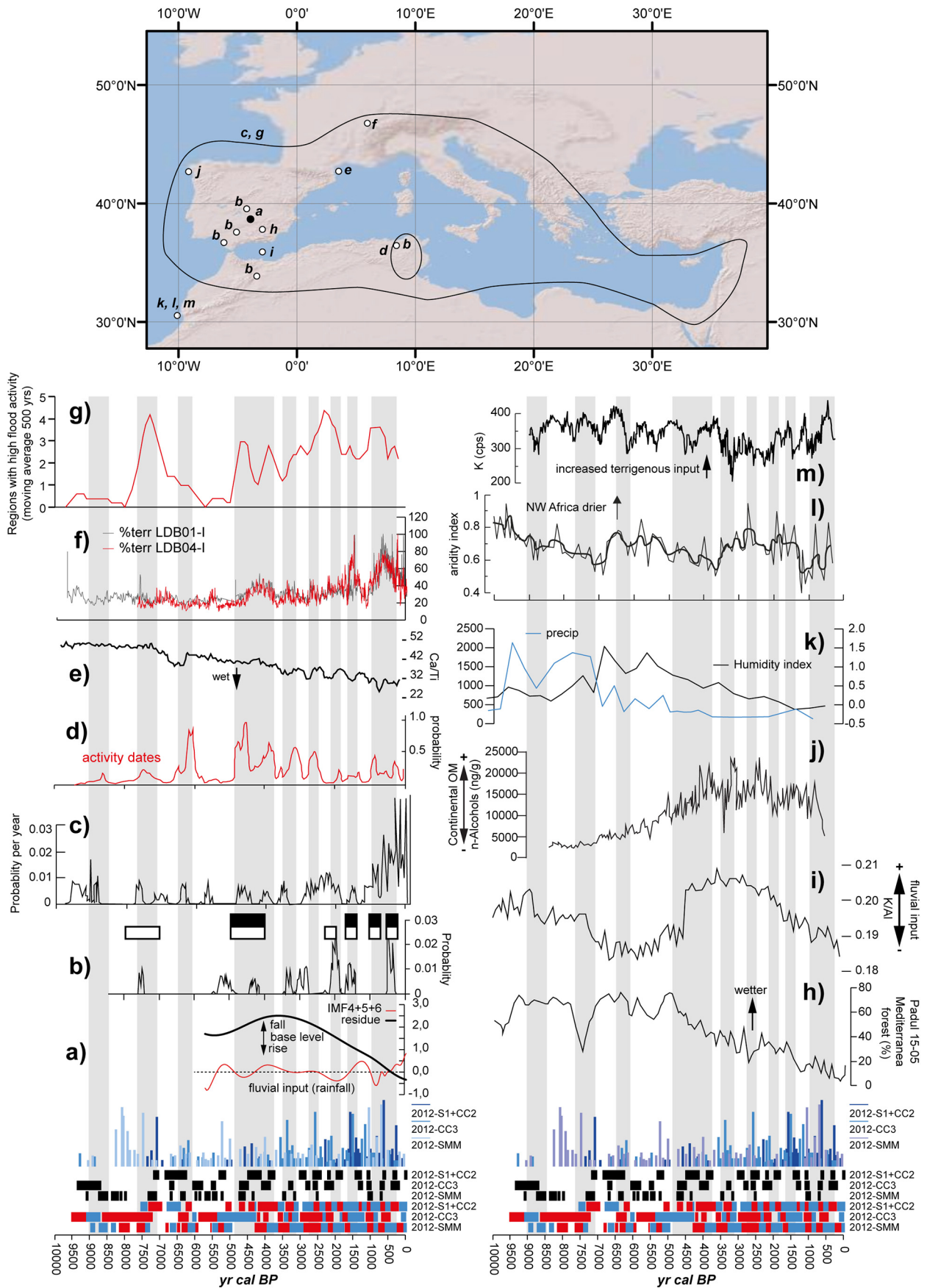


Fig. 8. Interpreted flood events from the geochemical information. For additional colour keys (environment, facies) see Fig. 7.



(caption on next page)

Fig. 9. Comparison of the observed high-water/flooding periods resulting from this study (bottom graphs, black bars: high sediment supply periods, red bars: low-water stages, blue bars: high-water stages) to other regional records. a) Intrinsic Mode Functions for the last 6000 years for the fluvial input in Las Tablas de Daimiel National Park (Guadiana River, Santisteban et al., 2017b); b) cumulative probability function for radiocarbon dates of the Jarama River (Faust and Wolf, 2017); c) summed probability for radiocarbon dating from slackwater deposits from Spanish (Atlantic + Mediterranean) rivers (Benito et al., 2008); d) periods of stability and activity for the Central Tunisia rivers (Zielhofer and Faust, 2008); e) Ca/Ti ratio for the sediments offshore of the Rhône River mouth indicative of wet/dry conditions (Bassetti et al., 2016); f) percentage of terrigenous material supplied to Lac Le Bourget (Arnaud et al., 2012); g) number of regions with increased river flooding in the European Mediterranean region (Benito et al., 2015b); h) humidity reconstruction from pollen data at Padul wetland (SE Spain, Ramos-Román et al., 2018); i) fluvial inputs recorded in the East Alborán Sea (core 293G, Rodrigo-Gámiz et al., 2011); j) continental OM inputs to Ría de Muros area (NW Spain, Pena et al., 2010); k) aridity index from NW Africa from marine core Geob7920-2 (Tjallingii et al., 2008) and precipitation index for NW Africa from leaf wax isotopes from marine cores (Tierney et al., 2017); l) aridity index for NW Africa from core Geob6007-2 (Moroccan margin; Holz et al., 2007); m) terrigenous input from core Geob6007 (Moroccan margin, Kuhlmann et al., 2004). Grey bars indicate common periods of flooding for the Western Mediterranean region. (For interpretation of the references to color in this figure legend, the reader is referred to the web version of this article.)

basin. Some regional events took place around 6300 cal. BP, 6000 cal. BP and 5500 cal. BP, while noticeable floods in the Guadiana-Azuer sub-basin occurred from 5300 to 5000 cal. BP. Regional flooding is also recorded towards the end of the fluvial sedimentation at downstream sections (cores 2012-S1 + CC2 and CC3) from 4300 to 4000 cal. BP, around 3100, 2600, 2200, from 700 to 1100 cal. BP, and during the 19th c. CE. Local flooding was important in the Guadiana-Azuer sub-basin at 3300 cal. BP and 500 cal. BP while the record shows flooding peaks for the Gigüela River from 1750 cal. BP to 1500 cal. BP (Fig. 8).

3.3. Upper Guadiana floods in the western Mediterranean context and global forcings

Fluvial records are very heterogeneous and, as stated above, their interpretation can change depending on how their spatial variability is interpreted. For this reason, they must be compared at different spatial scales to extract hints about the forcings controlling their evolution. There are no existing studies covering Holocene paleofloods in the upper Guadiana River basin and only few providing paleoclimate or paleohydrological records for a period longer than the documentary period (Dorado et al., 2002; Santisteban et al., 2017b) so comparisons must be done to other studies in the western Mediterranean area (Fig. 9).

These records are very heterogeneous as they cover a wide area, which means they capture diversity of local conditions, while the variety of proxies used mean proximal records can show obvious differences but also common features. There is a N-S gradient marked by different Holocene hydroclimate trends. A dry early Holocene changing to humid conditions is recorded by low fluvial inputs into lakes or marine basins that increase from mid-late Holocene until present at the Rhône River mouth (NW Mediterranean, Bassetti et al., 2016), Lake Bourget (Alps, Arnaud et al., 2012) and Ría de Muros (NW Spain, Pena et al., 2010). Around the southern Mediterranean, records show a wet climate during the early Holocene changing to arid conditions in NW Africa (Tjallingii et al., 2008; Tierney et al., 2017), the Alborán Sea (SW Mediterranean, Rodrigo-Gámiz et al., 2011), SE Spain (Padul wetland, Ramos-Román et al., 2018) and the upper Guadiana Basin (Dorado et al., 2002). This change is not synchronous across the northern margin, however, because a shift to wetter conditions took place after 7000 cal. BP at the Rhône River basin (Bassetti et al., 2016), after 4000 cal. BP at Lake Bourget (Arnaud et al., 2012), reaching maximum moisture in NW Spain around 3000 cal. BP (Pena et al., 2010). At the southern margin, the African Humid Period finished around 6000 cal. BP in NW Africa (Tjallingii et al., 2001; Tierney et al., 2017), and after 5000 cal. BP at the Alborán Sea (Rodrigo-Gámiz et al., 2011), SE Spain (Ramos-Román et al., 2018) and the upper Guadiana Basin (Dorado et al., 2002; Santisteban et al., 2017b). These features point towards a mid-Holocene reorganization of the climate (Wirtz et al., 2010) that affected the fluvial systems.

This record of flooding can be split in two periods, as noted by Zielhofer and Faust (2008) or Benito et al. (2015a, 2015b), marked by an increase in flooding frequency from 5500 to 4500 cal. BP onwards all around the western Mediterranean. Nevertheless, the mid-Holocene

climate reorganization means differences in the water budget evolution from north (to wetter) to south (to drier) are reflected in changes in the amount of sediment supplied by the rivers. There is a decrease in supply towards the south (Fig. 9i, j, m; Kuhlmann et al., 2004; Pena et al., 2010; Rodrigo-Gámiz et al., 2011) but an increase from more northerly rivers (Fig. 9e, f; Arnaud et al., 2012; Bassetti et al., 2016).

For the early Holocene period, at the upper Guadiana River basin, there are flood clusters around 9.7–9.3, 8.9, 7.1, 6.3, 6 and 5.5 ka cal. BP (this study) corresponding to both high and low water stages, while Dorado et al. (2002) identified fluvial activity (channels) ca. 9 and 8–7 ka cal. BP, coinciding with regional wet conditions. For rivers in central (Jarama River) and south Spain (Guadalete and Guadalquivir rivers), Wolf and Faust (2015) identified a fluvial aggradation episode around 8–7 ka cal. BP. However, Benito et al. (2008), after analysing the Spanish fluvial basins, found flooding clusters at 10.75–10.24, 9.55–9.13 ka cal. BP. In Tunisia, Zielhofer and Faust (2008) found fluvial aggradation at 6.2–6 ka cal. BP. All these episodes were linked to cold and dry conditions. Fluvial input into the Alborán Sea is characterized by low amplitude fluctuations that end with a drop from 7 to 4.5 ka cal. BP, before an abrupt rise at that time (Rodrigo-Gámiz et al., 2011). Near this area, the period 9.5–7.6 ka cal. BP period is considered the wettest of the Holocene, changing at that point to drier conditions (Ramos-Román et al., 2018). For NW Spain, Pena et al. (2010) found increased runoff periods for 8.1–7.8, 7.2–6.6, 5.7–5 ka cal. BP that related to the displacement of storm tracks during cold events in the Atlantic. At the Rhône River mouth, Bassetti et al. (2016) identified an episode of higher river supply at 8.2 ka cal. BP corresponding to a cold and wet pulse during an arid period. At Lake Bourget, Arnaud et al. (2012) found more frequent, but low intensity, floods at 9.4, 8.9, 8.6, 8.3, 8, 7.6, 6.8, 6, 5.7–5.4 ka cal. BP that they interpret as wet episodes during this arid phase in the Alps. On a Mediterranean scale, Benito et al. (2015a, 2015b) identify flood clusters at 9.5–9.2, 7.5–7 ka cal. BP and increased flooding activity at the Tagus River around 6.5–5.5 ka cal. BP but consider that synchrony for this period was poor. These authors linked this flooding to negative winter NAO and low irradiance periods.

After the mid-Holocene climate reorganization, floods become more frequent and intense. At the upper Guadiana River basin, Dorado et al. (2002) identify an aridity trend for the last 5 ka punctuated by arid episodes at 5 and 2.5 ka cal. BP. For this period, Santisteban et al. (2017b) find a rise of the base level for this period and pulses of fluvial sediment supply at ca. 5.2, ca. 3.8, 2.5, ca. 1.3 and an increase since 0.7 ka cal. BP. In this study, regional flooding (mainly during low water levels) from 4.3–4, ca. 3.1, 2.6, 2.2, 1.1–0.7 ka cal. BP, and during the 19th c. CE, while local flooding (both low and high-water stages) was important at 5.3–5, 3.3, 1.75–1.5 and 0.5 ka cal. BP. Fluvial activity also increased in central and south Spain, with aggradation episodes at 5–3.8, 2.2–1.5, ca. 1, ca. 0.4 ka cal. BP (Wolf and Faust, 2015), coincidental to cold and arid periods. For the largest Spanish fluvial basins, Benito et al. (2008) group floods into four clusters (4.82–4.44, 2.865–2.35, 0.96–0.79, 0.52–0.29 ka cal. BP) that they relate to cold periods and, for the last 3 ka, link to negative NAO conditions during winter.

Fluvial aggradation periods for Spain and Tunisia are placed at 4.6–3.8, 1.6, 1, 0.4 ka cal. BP (Faust and Wolf, 2017). These authors argue that, at the present moment, there is no well-established relation between these periods and climate, but they are more common during cold and dry episodes. Also for Tunisia, Zielhofer and Faust (2008) identified periods of great fluvial activity at 4.8–4.5, 4.1, 3.7, 3.3–3 ka cal. BP with a clear relation to climate (during cold and dry periods) since 4.8 ka cal. BP. Fluvial inputs into the Alborán Sea experienced a sudden rise at 4.5 ka cal. BP, reaching maximum values around 3.5 ka cal. BP, and then decreased until present (Rodrigo-Gámiz et al., 2011). They identify arid pulses, when fluvial activity was lower, at 6–4.5, 3.7–3.1, 2.6–2.3, 1.5–0.7 ka cal. BP and they link this wet/dry alternation to changes in the NAO (positive: arid, negative: wet) and in the Intertropical Convergence Zone, which causes the displacement of the African monsoon. This aridity trend is also observed for the last 5 ka in SE Spain (Padul wetland, Ramos-Román et al., 2018). At Ría de Muros (NW Spain), episodes of higher runoff to the estuary are dated to 3.8–3.2, 2.3–1.8, 1.3–1, 0.8–0.5 ka cal. BP that, as for older episode, could be related to displacements of the storm tracks during cold periods (Pena et al., 2010). At 7 ka cal. BP, moisture started to increase at the Rhône mouth (Bassetti et al., 2016). Increased fluvial supply took place at 6.6 to 4.4 ka cal. BP, under a mild and moist climate, at 2.84, 1.5, 0.72 ka cal. BP, during cold and wet spells, and 3.5, 2.2, 1 ka cal. BP, warm and dry episodes (Bassetti et al., 2016). In the Alpine domain, Lake Bourget, climate became wetter around 4 ka cal. BP and higher terrigenous inputs are recorded at 4.8–3.8, 3.2, 2.8, 2.4, 2.2, 1.9, 1.65–1.45, 1.45–1.3, 0.75–0.65 ka cal. BP, peaks at 1050, 900 cal. BP during more humid events (Arnaud et al., 2012).

Benito et al. (2015a,b) found that aridification increased from 5 ka cal. BP onwards and floods became more frequent and intense. They identify flooding episodes at the Mediterranean basin scale at 4.8–4.6, 4.1–3.7, 3.3–3.2, 2.85–2.75, 2.3–2.1, 1.7–1.6, 1.5–1.4, 0.95–0.8, ca. 0.3 and 0.2–0.1 ka cal. BP, contemporaneous to cold and wet periods. They consider that flooding is correlated to negative NAO during winter/autumn that favours the southward migration of the westerlies enhancing instability, storms and rainfall in the Mediterranean. They also consider that most flooding episodes coincide with low solar irradiance periods.

Considering all this records around western Mediterranean (including this study), there are common episodes at an interbasinal scale of flooding or higher fluvial sediment supply around 9000–8400 cal. BP, 7700–7100 cal. BP, 6400–6200 cal. BP, 4900–3700 cal. BP, 3500–3300 cal. BP, ca. 2600 cal. BP, ca. 2000 cal. BP, ca. 1500 cal. BP and 1000–300 cal. BP (more intense around 1000–700 cal. BP) (Fig. 9).

Most authors find a correlation between flooding, millennial-scale cold events related to North Atlantic dynamics (Zielhofer and Faust, 2008; Benito et al., 2008, 2015a, 2015b; Pena et al., 2010) and the NAO (negative periods enhancing intense rainfall) (Benito et al., 2008, 2015a,b; Rodrigo-Gámiz et al., 2011; Bassetti et al., 2016). A relation to solar activity has also been invoked, both in relation to changes in irradiance (Benito et al., 2015a) and solar activity (Peña and Schulte, 2014; Peña et al., 2015; Schulte et al., 2015). Changes in insolation have been invoked to explain the mid-Holocene reorganization of the climate system that affected the fluvial dynamics (Wirtz et al., 2010; Benito et al., 2015b; Ramos-Román et al., 2018). All these factors could have caused changes in the atmospheric gradients affecting the position of the storm tracks related to the westerlies (Benito et al., 2015a; Ramos-Román et al., 2018) or the trade winds (Rodrigo-Gámiz et al., 2011). However, Faust and Wolf (2017) performed a critical review of these factors and concluded that the complexity of fluvial dynamics means these assumptions must remain as hypotheses until the systems are better understood.

When we compare our record to the proposed common flooding periods and forcings, we observe several coincidences (Fig. 10). Regarding the bipartite division of the Holocene climate, the early Holocene period (less frequent and lower magnitude floods) corresponds to

higher interseason (summer-winter) (Fig. 10a upper) and S–N (30°N–46°N) summer gradients against low winter S–N gradients (Fig. 10a middle), while the mid-late Holocene (more frequent and intense floods) correlates to lower interseason and S–N summer gradients, and higher S–N winter gradients.

Increasing the time resolution (millennial to centennial scales), the less frequent flooding periods correspond to nodes in the insolation curves (Fig. 10a lower) while the period with more frequent flood episodes coincides with the antinodes (high winter insolation and low summer insolation). The first situation correlates to minima in irradiance (Fig. 10b) and colder temperatures in the North Atlantic (Fig. 10d), while the second situation coincides with maxima in irradiance and warmer summer North Atlantic SST.

However, there is no consistent relationship with the NAO (Fig. 10c). There are hints that lower NAO values correspond to higher flood frequencies during the interval 4.5 ka cal. BP to 1.5 ka cal. BP, while flood frequencies increase for the last 1.5 ka when NAO values are higher than previously.

When examined at a resolution of decades to centuries, and considering the uncertainty related to the flood chronologies, widespread flooding periods align with reduced irradiance, colder North-Atlantic SST and it seems that there is a better correlation to negative NAO values. However, this correlation is not universal as not all negative NAO periods coincide with flooding episodes.

For the long-term Holocene sequence, the higher summer gradient during the early Holocene (Fig. 10a, middle) correlates to high summer and low winter insolation values (Fig. 10a lower), which is coherent with a strengthening of the Hadley Cell and a northward displacement of the zonal winds. This could be responsible for the wetter south Mediterranean and a dry north Mediterranean.

But from 5 ka cal. BP onwards, the seasonal contrast (Fig. 10a upper) reached its minimum, the summer insolation was also at its minima and the winter insolation at its maxima. This meant the spatial gradients for summer decreased while the gradient for winter was the greatest for the Holocene. This situation flips the earlier conditions and caused the southward displacement of the wind systems, bringing moisture to the north Mediterranean and aridity to the south Mediterranean. The dominance of the inter- (seasonal gradients) or intra-annual (spatial gradients and absolute values) variability in insolation and the combined effect with shorter term changes in irradiation (changing the energy budget or the evaporation) and atmosphere-ocean teleconnections (i.e. negative winter NAO causing the southward displacement of the westerlies) could have been favoured the higher frequency paleohydrological fluctuations responsible for the mid-late Holocene flooding periods. However, as Faust and Wolf (2017) stated, many unknowns persist when linking rivers and climate systems and uncertainties in our knowledge about fluvial systems (environmental, chronological, etc.) means these findings must be treated cautiously and cannot be taken as firm conclusions.

4. Conclusions

To reconstruct the Holocene fluvial history of the upper Guadiana River basin, it has been necessary to understand the variability of the system (environmental dynamics and products) to develop a set of sedimentological and geochemical proxies that identify different hydrological changes related to flooding. Then, a comparison of different points in the basin allow these changes to be interpreted as internal variability (autocyclic) or the result of external forcings (alloycyclic), which can then be compared to records in other basins.

Analysis of local vs. basin-wide changes and their spatial homogeneity, trend analysis, and use of different sets of proxies related to the features of the sedimentary system are tools that help in the development of a hierarchy of flood events in time (single events, periods, trends of events) and space (local, regional, inter-basinal). Combining facies and facies sequences with proxies of fluvial energy that may be

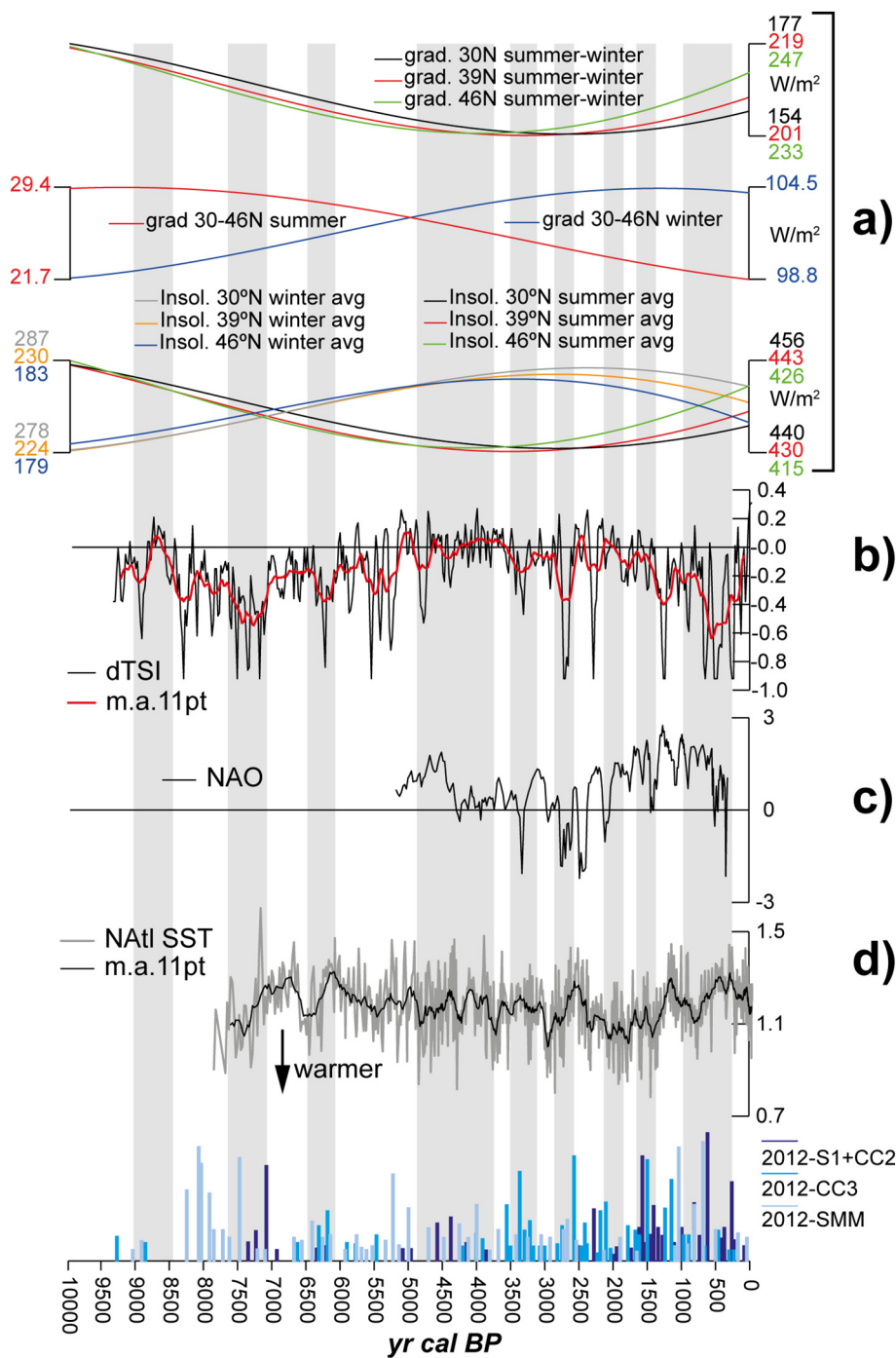


Fig. 10. Comparison of the observed high-water/flooding periods resulting from this study (bottom graphs) to some external forcings: a) upper: summer-winter insolation gradient (from 14 to 23 W/m²), middle: 30°N–46°N insolation gradient for summer and winter (in both cases around 5.7 W/m²), lower: time-averaged insolation (W/m²) curves for summer (range variation from 11 to 16 W/m²) and winter (range variation from 4 to 9 W/m²) at 30°N (Canary Islands), 39°N (study area) and 46°N (Lake Bourget) (calculated using the R package ‘palinsol’, Crucifix, 2016, using the calculations of Berger and Loutre, 1991); b) difference of total solar irradiance (dTSl) from the value of the PMOD composite during the solar cycle minimum of the year 1986 CE in W/m² (Steinhilber et al., 2012); c) NAO reconstruction for the last 5000 years (Olsen et al., 2012); d) δ¹⁸O of Neogloboquadrina pachyderma (dex) (a proxy for North Atlantic summer SST -Natl SST-, Sejrup et al., 2011). m.a. 11 pt: moving average, 11 points.

sensitive to high frequency changes is a good starting point for this kind of analysis.

Comparison of this flood record to similar reconstructions around the western Mediterranean shows a set of common flooding periods at 9000–8400 cal. BP, 7700–7100 cal. BP, 6400–6200 cal. BP, 4900–3700 cal. BP, 3500–3300 cal. BP, ca. 2600 cal. BP, ca. 2000 cal. BP, ca. 1500 cal. BP and 1000–300 cal. BP. The distribution in time and space of these centennial to millennial-scale flooding periods could be related to changes in orbital insolation and its interannual, intra-annual and spatial variability.

The complexity of the hydrological settings, our limited understanding of the long-term dynamics of the fluvial systems, and uncertainties about their environmental interpretation and chronologies preclude drawing higher-resolution inferences. However, it seems

reasonable to consider that atmospheric and oceanographic teleconnections, together with external changes (i.e. irradiance), could have been connected to the shorter flooding episodes.

5. Acknowledgements

This research has been funded by a research grant of the Ministry of Economy and Competitiveness (CGL2011-30302-C02-01) and it's a contribution to IGCP-618. The authors are grateful to the Geological Survey of Spain and the University of Barcelona for their help in using the XRF core scanners. The authors are grateful to the two anonymous reviewers whose valuable comments have improved this manuscript. We are also grateful to the editors of this special issue for their help and support. Special thanks are due to Daniel Schillereff for helping with the

language editing.

References

- Allanson, B.R., Hart, R.C., O'Keefe, J.H., Robarts, R.D., 1990. Inland Waters of Southern Africa: An Ecological Perspective. Monographiae Biologicae. Kluwer Academic Publishers, Dordrecht, Boston, London, pp. 64.
- Arnaud, F., Révillon, S., Debret, M., Revel, M., Chapron, E., Jacob, J., Giguet-Covex, C., Poulenard, J., Magny, M., 2012. Lake Bourget regional erosion patterns reconstruction reveals Holocene NW European Alps soil evolution and paleohydrology. *Quat. Sci. Rev.* 51, 81–92.
- Bassetti, M.A., Berné, S., Sicre, M.A., Dennielou, B., Alonso, Y., Buscail, R., Jalali, B., Hebert, B., Menniti, C., 2016. Holocene hydrological changes in the Rhône River (NW Mediterranean) as recorded in the marine mud belt. *Clim. Past* 12, 1539–1553.
- Benito, G., Thorndycraft, V.R., Rico, M., Sánchez-Moya, Y., Sopena, A., 2008. Palaeoflood and floodplain records from Spain: evidence for long-term climate variability and environmental changes. *Geomorphology* 101, 68–77.
- Benito, G., Macklin, M.G., Panin, A., Rossato, S., Fontana, A., Jones, A.F., Machado, M.J., Matkhova, E., Mozzi, P., Zielhofer, C., 2015a. Recurring flood distribution patterns related to short-term Holocene climatic variability. *Sci. Rep.* 5, 16398. <https://doi.org/10.1038/srep16398>.
- Benito, G., Macklin, M.G., Zielhofer, C., Jones, A.F., Machado, M.J., 2015b. Holocene flooding and climate change in the Mediterranean. *Catena* 130, 13–33.
- Berger, A., Loutre, M.E., 1991. Insolation values for the climate of the last 10 million years. *Quat. Sci. Rev.* 10, 297–317.
- Bradley, C., 1997. The hydrological basis for conservation of floodplain wetlands: implications of work at Narborough Bog, UK. *Aquat. Conserv. Mar. Freshwat. Ecosyst.* 7, 41–62.
- Calvert, S.E., Pedersen, T.F., 2007. Elemental proxies for palaeoclimatic and palaeoceanographic variability in marine sediments: interpretation and application. In: Hillaire-Marcel, C., De Vernal, A. (Eds.), *Proxies in Late Cenozoic Paleoclimatology*, Developments in Marine Geology. 1. Elsevier, Amsterdam, Boston, Heidelberg, London, pp. 567–644.
- Carignan, R., Neiff, J.J., 1992. Nutrient dynamics in the floodplain ponds of the Paraná River (Argentina) dominated by the water hyacinth *Eichhornia crassipes*. *Biogeochemistry* 17, 85–121.
- Celis, A., Mediavilla, R., Santisteban, J.I., Castaño, S., de la Losa, A., 2017. La desecación de las Tablas de Daimiel (1750-1987): cambios agrarios e impactos medioambientales a partir de la interpretación del registro sedimentario. *Historia Agraria* 71, 5–35.
- Crucifix, M., 2016. Palinsol: Insolation for Palaeoclimate Studies. R Package Version 0.93. <https://CRAN.R-project.org/package=palinsol>.
- de Bustamante, I., Dorado, M., Rojas, B., Temiño, J., Segura, M., García-Hidalgo, J.F., Pérez, P., Valdeolmillos, A., Sicilia, F., Fernández, I., López, M.J., 1995. Análisis del impacto ambiental de la explotación de los depósitos de turba asociados al río Guadiana en la Llanura Manchega e interés de su conservación. Informe Final del Proyecto Fundación Ramón Areces-Universidad de Alcalá, Alcalá de Henares, pp. 125.
- Dhivert, E., Grosbois, C., Coynel, A., Lefèvre, I., Desmet, M., 2015. Influences of major flood sediment inputs on sedimentary and geochemical signals archived in a reservoir core (Upper Loire Basin, France). *Catena* 126, 75–85.
- Domínguez-Castro, F., Santisteban, J.I., Mediavilla, R., Dean, W.E., López-Pamo, E., Gil-García, M.J., Ruiz-Zapata, M.B., 2006. Environmental and geochemical record of human-induced changes in C storage during the last millennium in a temperate wetland (Las Tablas de Daimiel National Park, central Spain). *Tellus B* 58, 573–585.
- Dorado, M., Valdeolmillos, A., Ruiz Zapata, M.B., Gil García, M.J., Bustamante, I., 2002. Climatic changes since the late glacial/Holoceno transition in the Mancha plain (South Central Iberian Peninsula, Spain) and their evidence in Las Tablas Daimiel marshlands. *Quat. Int.* 93–94, 73–84.
- European Union, 2007. Directive 2007/60/EC of the European Parliament and of the Council of 23 October 2007 on the assessment and management of flood risks. *Off. J. Eur. Union* 2007. L 288/27, 6.11. <https://eur-lex.europa.eu/legal-content/EN/TXT/HTML/?uri=CELEX:32007L0060&from=EN>.
- Faust, D., Wolf, D., 2017. Interpreting drivers of change in fluvial archives of the Western Mediterranean - a critical view. *Earth Sci. Rev.* 174, 53–83.
- Hamilton, S.K., Lewis Jr., W.M., 1990. Basin morphology in relation to chemical and ecological characteristics of lakes on the Orinoco River floodplain. *Venezuela. Archiv für Hydrobiologie* 119, 393–425.
- Hartmann, D.L., Klein Tank, A.M.G., Rusticucci, M., Alexander, L.V., Brönnimann, S., Charabi, Y., Dentener, F.J., Dlugokencky, E.J., Easterling, D.R., Kaplan, A., Soden, B.J., Thorne, P.W., Wild, M., Zhai, P.M., 2013. Observations: atmosphere and surface. In: Stocker, T.F., Qin, D., Plattner, G.-K., Tignor, M., Allen, S.K., Boschung, J., ... Midgley, P.M. (Eds.), *Climate Change 2013: The Physical Science Basis. Contribution of Working Group I to the Fifth Assessment Report of the Intergovernmental Panel on Climate Change*. Cambridge University Press, Cambridge, United Kingdom and New York, NY, USA, pp. 159–254.
- Heery, S., 1993. The Shannon Floodlands: A Natural History of the Shannon Callows. Tír Eolas. Kinvara, Ireland.
- Hernández, P., Huerta, J., López, F., Portero, J.M., Solesio, J., Gil, D., Pérez, A., 2013. Mapa Geológico de España E. 1:50000 Hoja 18–29 Malagón. Servicio de Publicaciones Instituto Geológico y Minero de España, Madrid.
- Hesse, P.P., Williams, R., Ralph, T.J., Fryirs, K.A., Larkin, Z.T., Westaway, K.E., Farebrother, A., 2018. Palaeohydrology of lowland rivers in the Murray-Darling Basin, Australia. *Quat. Sci. Rev.* 200, 85–105.
- Holz, C., Stuut, J.-B.W., Henrich, R., Meggers, H., 2007. Variability in terrigenous sedimentation processes off Northwest Africa and its relation to climate changes: inferences from grain-size distributions of a Holocene marine sediment record. *Sediment. Geol.* 202, 499–508.
- Jiménez Cisneros, B.E., Oki, T., Arnell, N.W., Benito, G., Cogley, J.G., Döll, P., Jiang, T., Mwakalila, S.S., 2014. Freshwater resources. In: Field, C.B., Barros, V.R., Dokken, D.J., Mach, K.J., Mastrandrea, M.D., Bilir, T.E. ... White, L.L. (Eds.), *Climate Change*. vol. 2014. *Global and Sectoral Aspects. Contribution of Working Group II to the Fifth Assessment Report of the Intergovernmental Panel on Climate Change*. Cambridge University Press, Cambridge, United Kingdom and New York, NY, USA, Impacts, Adaptation, and Vulnerability. Part A, pp. 229–269.
- John, D.M., 1986. The Inland Waters of Tropical West Africa: An Introduction and Botanical Review. *Archiv für Hydrobiologie: Ergebnisse der Limnologie Heft.* vol. 23 Schweizerbart Science Publishers, Stuttgart, Germany.
- Junk, W.J., 1984. Ecology of the várzea, Amazonian whitewater rivers. In: Sioli, H. (Ed.), *The Amazon*. Monographiae Biologicae, 56. Springer, Dordrecht, pp. 215–243.
- Köhler, J., 1993. Growth, production and losses of phytoplankton in the lowland River Spree. I. Population dynamics. *J. Plankton Res.* 15, 335–349.
- Kuhlmann, H., Meggers, H., Freudenthal, T., Wefer, G., 2004. The transition of the monsoonal and the N Atlantic climate system off NW Africa during the Holocene. *Geophys. Res. Lett.* 31, L22204.
- Larkin, Z.T., Ralph, T.J., Tooth, S., McCarthy, T.S., 2017. The interplay between extrinsic and intrinsic controls in determining floodplain wetland characteristics in the South African drylands. *Earth Surf. Process. Landf.* 42, 1092–1109.
- Lewin, J., Ashworth, P.J., 2014. The negative relief of large river floodplains. *Earth Sci. Rev.* 129, 1–23.
- McCarthy, T.S., Tooth, S., Jacobs, Z., Rowberry, M.D., Thompson, M., Brandt, D., Hancox, P.J., Marren, P.M., Woodborne, S., Ellery, W.N., 2011. The origin and development of the Nyl River floodplain wetland, Limpopo Province, South Africa: trunk–tributary river interactions in a dryland setting. *S. Afr. Geogr. J.* 93, 172–190.
- Mediavilla, R., Santisteban, J.I., Mediató, J.F., 2013. El registro sedimentario del Holoceno en el Parque Nacional de Las Tablas de Daimiel. In: Mediavilla, R., Instituto Geológico y Minero de España, Serie: Medio Ambiente (Eds.), *Las Tablas de Daimiel: Agua y sedimentos*. Publicaciones del. vol. 14. IGME, Madrid, pp. 169–186.
- Mertes, L.A.K., 1997. Documentation and significance of the perirheic zone on inundated floodplains. *Water Resour. Res.* 33, 1749–1762.
- Middleton, G., 1973. Johannes Walther's Law of correlation of facies. *Geol. Soc. Am. Bull.* 38, 979–988.
- Olsen, J., Anderson, N.J., Knudsen, M.F., 2012. Variability of the North Atlantic Oscillation over the past 5,200 years. *Nat. Geosci.* 5, 808–812.
- Ohta, T., 2008. Measuring and adjusting the weathering and hydraulic sorting effects for rigorous provenance analysis of sedimentary rocks: a case study from the Jurassic Ashikita Group, south-West Japan. *Sedimentology* 55, 1687–1701.
- Pena, L.D., Francés, G., Diz, P., Esparza, M., Grimalt, J.O., Nombela, M.A., Alejo, I., 2010. Climate fluctuations during the Holocene in NW Iberia: high and low latitude linkages. *Cont. Shelf Res.* 30, 1487–1496.
- Peña, J.C., Schulte, L., 2014. Effects of solar activity and climate variability on large floods in Switzerland. *Boletín de la Asociación de Geógrafos Españoles* 65, 469–475.
- Peña, J.C., Schulte, L., Badoux, A., Barriados, M., Barrera-Escoda, A., 2015. Influence of solar forcing, climate variability and modes of low-frequency atmospheric variability on summer floods in Switzerland. *Hydrol. Earth Syst. Sci.* 19, 3807–3827.
- Portero, J.M., Ramírez, J.I., Gallardo Díaz, J., Aguilar, M.J., Ancochea, E., Leal, M.C., Molina, E., Pérez González, A., 1988. Mapa Geológico de España E. 1:50000 Hoja 19–30 Daimiel. Servicio de Publicaciones Instituto Geológico y Minero de España, Madrid.
- Ramos-Román, M.J., Jiménez-Moreno, G., Camuera, J., García-Alix, A., Anderson, R.S., Jiménez-Espejo, F.J., Sachse, D., Toney, J.L., Carrión, J.S., Webster, C., Yanes, Y., 2018. Millennial-scale cyclical environment and climate variability during the Holocene in the western Mediterranean region deduced from a new multiproxy analysis from the Padul record (Sierra Nevada, Spain). *Glob. Planet. Chang.* 168, 35–53.
- Reimer, P.J., Bard, E., Bayliss, A., Beck, J.W., Blackwell, P.G., Bronk Ramsey, C., Buck, C.E., Cheng, H., Edwards, R.L., Friedrich, M., Grootes, P.M., Guilderson, T.P., Haffidason, H., Hajdas, I., Hatte, C., Heaton, T.J., Hoffmann, D.L., Hogg, A.G., Hughen, K.A., Kaiser, K.F., Kromer, B., Manning, S.W., Niu, M., Reimer, R.W., Richards, D.A., Scott, E.M., Southon, J.R., Staff, R.A., Turney, C.S.M., van der Plicht, J., 2013. IntCal13 and Marine13 radiocarbon age calibration curves 0–50,000 years cal BP. *Radiocarbon* 55, 1869–1887.
- Rey, J., Martínez, J., Mediavilla, R., Santisteban, J.I., Castaño, S., de la Losa, A., 2017. Geophysical characterization of stratigraphical surfaces: Basin floor and sedimentological architectural elements of Las Tablas de Daimiel (Quaternary of southern-central Spain). *J. Appl. Geophys.* 136, 387–399.
- Richardson, C.J., Reiss, P., Hussain, N.A., Alwash, A.J., Pool, D.J., 2005. The Restoration potential of the Mesopotamian Marshes of Iraq. *Science* 307, 1307–1311.
- Rodrigo-Gámiz, M., Martínez-Ruiz, F., Jiménez-Espejo, F.J., Gallego-Torres, D., Nieto-Moreno, V., Romero, O., Ariztegui, D., 2011. Impact of climate variability in the western Mediterranean during the last 20,000 years: oceanic and atmospheric responses. *Quat. Sci. Rev.* 30, 2018–2034.
- Rodríguez-García, J.A., 1998. Geomorfología de Las Tablas de Daimiel y del endorreísmo manchego centro-occidental. M.Sc. Thesis (unpublished. Universidad Complutense de Madrid, Madrid).
- Santisteban, J.I., Mediavilla, R., 2013. Evolución de las temperaturas y precipitaciones desde el siglo XIX. In: Mediavilla, R., Instituto Geológico y Minero de España, Serie: Medio Ambiente (Eds.), *Las Tablas de Daimiel: Agua y sedimentos*. Publicaciones del. vol. 14. IGME, Madrid, pp. 17–36.
- Santisteban, J.I., Mediavilla, R., López-Pamo, E., Dabrio, C.J., Ruiz-Zapata, M.B., Gil-

- García, M.J., Castaño, S., Martínez-Alfaro, P.E., 2004. Loss on ignition: a qualitative or quantitative method for organic matter and carbonate mineral content in sediments? *J. Paleolimnol.* 32, 287–299.
- Santisteban, J.I., Mediavilla, R., Galán, L., Mediato, J.F., del Moral, B., 2017a. Palaeohydrological fluctuations for the last 25000 years as recorded in fluvial sediments of the Guadiana River (central Spain). In: PAGES 5th Open Science Meeting, Abstract Book, pp. 380–381.
- Santisteban, J.I., Mediavilla, R., Celis, A., Castaño, S., de la Losa, A., 2017b. Millennial-scale cycles of aridity as a driver of human occupancy in central Spain? *Quat. Int.* 407, 96–109.
- Schulte, L., Peña, J.C., Carvalho, F., Schmidt, T., Julià, R., Llorca, J., Veit, H., 2015. A 2600-year history of floods in the Bernese Alps, Switzerland: frequencies, mechanisms and climate forcing. *Hydrol. Earth Syst. Sci.* 19, 3047–3072.
- Sejrup, H.P., Hafliðason, H., Andrews, J.T., 2011. A Holocene North Atlantic SST record and regional climate variability. *Quat. Sci. Rev.* 30, 3181–3195.
- Steinhilber, F., Abreu, J.A., Beer, J., Brunner, I., Christl, M., Fischer, H., Heikkilä, U., Kubik, P.W., Mann, M., McCracken, K.G., Miller, H., Miyahara, H., Oerter, H., Wilhelms, F., 2012. 9,400 years of cosmic radiation and solar activity from ice cores and tree rings. *Proc. Natl. Acad. Sci.* 109, 5967–5971.
- Stuiver, M., Reimer, P.J., 1986. A computer program for radiocarbon age calibration. *Radiocarbon* 28, 1022–1030.
- Stuiver, M., Reimer, P.J., 1993. Extended ¹⁴C database and revised CALIB radiocarbon calibration program. *Radiocarbon* 35, 215–230.
- Stuiver, M., Reimer, P.J., Reimer, R., 2015. CALIB Radiocarbon Calibration Version 7.1. Available at: <http://calib.qub.ac.uk/calib/>.
- Tierney, J.E., Pausata, F.S.R., de Menocal, P.B., 2017. Rainfall regimes of the Green Sahara. *Sci. Adv.* 3 (1), e1601503. <https://doi.org/10.1126/sciadv.1601503>. <http://advances.sciencemag.org/content/3/1/e1601503>.
- Tjallingii, R., Claussen, M., Stuut, J.-B.W., Fohlmeister, J., Jahn, A., Bickert, T., Lamy, F., Röhl, U., 2008. Coherent high- and low-latitude control of the northwest African hydrological balance. *Nat. Geosci.* 1, 670–675.
- Tooth, S., McCarthy, T.S., 2007. Wetlands in drylands: geomorphological and sedimentological characteristics, with emphasis on examples from southern Africa. *Prog. Phys. Geogr.* 31, 3–41.
- Valdeolmillos, A., 2005. *Registro paleoclimático y paleoambiental de los últimos 350000 años en el Parque Nacional de Las Tablas de Daimiel (Ciudad Real)*. PhD Thesis. Universidad de Alcalá. In: Alcalá de Henares, pp. 308.
- Viscosi-Shirley, C., Mammone, K., Piasias, N., Dymond, J., 2003. Clay mineralogy and multi-element chemistry of surface sediments on the Siberian-Arctic shelf: implications for sediment provenance and grain size sorting. *Cont. Shelf Res.* 23, 1175–1200.
- Walther, J., 1894. Einleitung in die Geologie als historische Wissenschaft. In *Lithogenesis der Gegenwart*. Jena: G. Fischer 3, 535–1055.
- Winter, T.C., 1999. Relation of streams, lakes, wetlands to groundwater flow systems. *Hydrogeol. J.* 7, 28–45.
- Wirtz, K.W., Lohmann, G., Bernhardt, K., Lemmen, C., 2010. Mid-Holocene regional reorganization of climate variability: analyses of proxy data in the frequency domain. *Palaeogeogr. Palaeoclimatol. Palaeoecol.* 298, 189–200.
- Wolf, D., Faust, D., 2015. Western Mediterranean environmental changes: evidences from fluvial archives. *Quat. Sci. Rev.* 122, 30–50.
- Zielhofer, C., Faust, D., 2008. Mid- and late Holocene fluvial chronology of Tunisia. *Quat. Sci. Rev.* 27, 580–588.